Structural determination of crystalline silicon by extended energy-loss fine-structure spectroscopy

M. De Crescenzi,* L. Lozzi, P. Picozzi, and S. Santucci
Dipartimento di Fisica, Università dell'Aquila, 67100 l'Aquila, Italy

M. Benfatto and C. R. Natoli
Istituto Nazionale di Fisica Nucleare, Laboratori Nazionali di Frascati, P.O. Box 13, 00044 Frascati, Italy
(Received 13 July 1988; revised manuscript received 21 December 1988)

We present recent structural results obtained through extended energy-loss fine-structure (EELFS) spectroscopy in the reflection mode above the silicon K edge. Although the electron-energy-loss technique is one of the most ancient tools for surface investigation, only recently has it been proved also to give local structural information. Thanks to an increased amount of experimental evidence, the physical process underlying the EELFS features, described in terms of a final-state interference effect similar to what happens in extended x-ray-absorption fine-structure (EXAFS) spectroscopy, seems to be well accepted now, although a deeper theoretical analysis is required. In this paper we compare EELFS and EXAFS features detected above the same edge in order to demonstrate that the dipole approximation can be applied with confidence even for a deep edge of ionization energy comparable with the primary beam energy. The good agreement between the structural parameters obtained by means of x rays and by low-energy primary electrons is theoretically explained in terms of a complete calculation of the inelastic-electron-scattering cross section. The most important result of this approach, based on the distorted-wave Born approximation, is the strong predominance of the dipole channel over the monopole and quadrupole contributions, at least for nodeless core initial wave functions. The present theory allows one to include in a manageable way multiple scattering and exchange effects.

INTRODUCTION

In the past few years EELFS (extended energy-loss fine-structure) technique has been proved to be a valuable tool for local structural investigation of clean surfaces and chemisorbed species.[1-4] The most attractive aspect of this technique is that the data analysis follows the procedure used for EXAFS (extended x-ray-absorption fine-structure) spectroscopy.[5-7] The great advantage and usefulness of the EXAFS technique lies in the simplicity of the theoretical formula for determining neighbor distances and structural parameters.

The oscillatory structure in an x-ray absorption spectrum $\mu(E)$ from a core level [schematically shown in Fig. 1(a)] is caused by a final-state interference effect between the excited electronic wave coming out from the absorbing atom and the backscattered part of this wave due to the presence of the surrounding atoms. Sayers, Stern, and Lytle[8] in order to fit this structure have suggested the following equation:

$$\chi(k)=\frac{N\tilde{A}(k,\pi)}{kR^2}\sin[2kR+\phi(k)]e^{-2\sigma^2k^2}e^{-2R/\lambda(k)}, \quad (1)$$

where k is the photoelectron wave vector, R is the neighbor-shell distance with coordination number N and backscattering amplitude $\tilde{A}(k,\pi)$, $\phi(k)$ is the phase shift experienced by the photoelectron in the emission-backscattering process, σ^2 is related to the thermal and static disorder, and $\lambda(k)$ is the mean free path of the excited core electron. For simplicity in Eq. (1) summation over different shells has been omitted.

Because the EXAFS spectroscopy needs mainly high-flux synchrotron radiation facilities, our purpose has been to demonstrate that an alternative similar structural technique is possible if one looks at the extended features present in the inelastic cross section $N(E)$ of the scattered electrons from a solid surface[9] [Fig. 1(b)]. Numerous works have been published to demonstrate the applicability of the EELFS technique in the determination of the structure of different compounds[9,10] and different metals deposited on clear surfaces.[11-13]

The focal point underlying the EELFS analysis is the assumption of the validity of the dipole approximation because it reduces the complexity of the functional form used to fit the experimental data. This approximation is generally well accepted for transmission energy-loss spectra[14-16] while its applicability for spectra carried out in the reflection mode should be in principle questionable because the primary beam has energy comparable with the energy losses.

In this work we report a complete study performed on a clean silicon surface using the EELFS technique in a reflection mode. We have chosen silicon because it is one of the most interesting elements from the point of view of both electronic properties and the technological applications. Moreover a fairly large amount of EXAFS and

surface EXAFS data of crystalline and amorphous silicon have been reported in the literature.[17–19]

The aim of our work can be summarized as follows: (a) to make a comparison between the EELFS structural information (radial distribution function, backscattering amplitude, and phase shift) and the one obtained by means of the EXAFS technique, (b) to evaluate the contribution of multiple plasmons on EELFS spectra which should be important when an electron probe is used to excite inner shell electrons, and (c) to compute the differential scattering cross section (above the silicon K edge) in such a way as to assess the relative weights of the various angular-momentum final-state channels.

These calculations, originally suggested by Leapmann *et al.* for the case of transmission energy-loss spectra[20] for a wide variety of inner shells of different atoms, are of crucial importance to show whether the dipole approximation is a valid and correct method of analysis of the extended energy-loss fine structure in the reflection mode.

In this latter mode however, as will be shown in Sec. IV of the paper, the validity of the Born approximation is highly questionable, since for intensity reason, the incident electron energy should be as low as 2–3 keV. The price to be paid is therefore a more complex theory, due to the much stronger elastic scattering of the incident beam of electrons at these energies and due to exchange effects between the projectile and the localized electrons of the system under study.

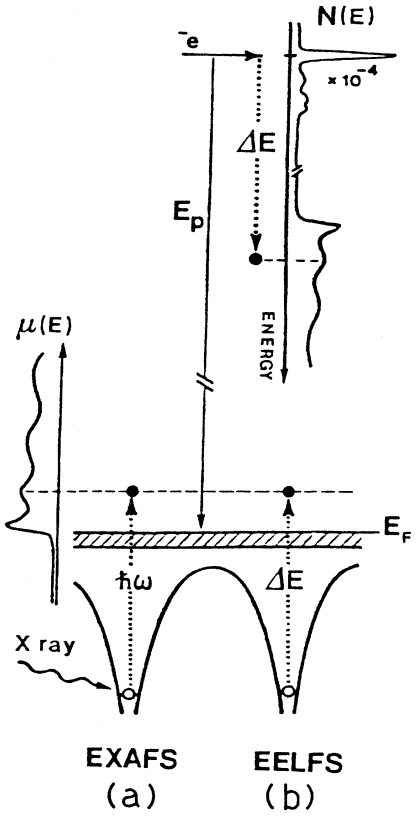

FIG. 1. Schematic pictures of (a) EXAFS and (b) EELFS processes. The modulation observed in the x-ray absorption coefficient $\mu(E)$ should correspond to the features observed in the yield $N(E)$ due to the back diffused electrons from a solid sample. In the EXAFS spectroscopy the different final states of the excited core electron above E_F may be filled by varying the energy $\hbar\omega$ of the x-ray probe. In the EELFS spectroscopy the same features are detected in $N(E)$ measuring different energy losses ΔE of the primary electron beam E_p which reflects the same final states of the core electron excited in the medium.

The first attempt at such a theory was that of Mila and Noguera[21] who treated the exchange and elastic scattering in what substantially is a distorted-wave Born approximation (DWBA), but taking the single-scattering approximation for the initial- and final-state electron wave functions.

However, due to the complexity of the resulting expression, the whole question of the validity of an approximate selection rule was left to a further investigation. The problem of the calculation of the Coulomb matrix element in the DWBA was taken up by Mehl and Einstein[22] with the aim to understand and analyze the extended fine structure found in the appearance potential spectroscopy. They presented evidence of two approximate selection rules by an incident electron, over the energy range of relevance to absorption structure experiments. The first approximate selection rule states that the dipole part of the Coulomb interaction dominates the ionization process at all energies of the "scattered" electron (the one with high energy in the final state; the "excited" electron is instead fixed at the ionization edge). The second approximate rule says that the dominant channel of the interaction is one in which the two final-state electrons both have angular momentum $l_c \pm 1$, where l_c is the angular momentum of the core electron.

Combined with the approach of Mila and Noguera,[21] the result of Mehl and Einstein would seem to ensure a substantial predominance of the $l_c + 1$ channel, provided it could be extrapolated to higher energies of the excited electron. It is difficult, however, to estimate the influence of all the other channels present in the final state in the structural analysis of the data, since their percent contribution can be as high as 80%.

A different approach was presented by Saldin[23] who treated the full multiple scattering of the projectile both *before* and *after* the inelastic scattering in a low-energy electron diffraction (LEED) formalism. However the final-state wave function of the lower energy excited electron was left unspecified. This approach made possible a convenient classification of the projectile scattering paths, from which it was possible to deduce that under the condition $\Delta\varepsilon/\varepsilon_i \ll 1$ for the primary beam, $\Delta\varepsilon$ being the energy loss and ε_i the incident energy of the projectile, the dominant paths involve elastic backscattering and small-angle inelastic scattering, which offers an explanation for the apparent dominance of the dipole-allowed channel in the atomic excitation process.

All this is well suited for systems consisting of a disordered low-Z atomic adsorbate on a crystal surface, where the condition $\Delta\varepsilon/\varepsilon_i \ll 1$ can easily be realized. Absorption from outer shells of medium Z adsorbates is another possible case. However, in the majority of cases, experimental conditions and detectability requirements do not

allow the realization of the condition $\Delta\varepsilon/\varepsilon_i \ll 1$. In all these instances the formulation of a general theory describing both the incident and the excited electrons in the correct and complete way would be highly useful. Such a theory is presented here and embodies the advantages of both approaches described above in a formulation which is not more complicated than that given by Saldin.[23] By explicitly evaluating the atomic radial transition-matrix elements M_l^0 [see Eq. (31) of the present paper] we in fact verify a predominance of the dipole component, at least for absorption from a K edge (nodeless function).

It is also shown that, in general, cross terms of the type $M_l \chi_n^{ll'} M_{l'}$ with different final l values, where $\chi_n^{ll'}$ $(n>2)$ represent the nth multiple-scattering contributions in which the final-state excited electron of lower energy leaves the excited atom with l angular momentum and returns to it with l', are not entirely negligible. These terms are important if $l=0$ and $l'=1$ and vice versa and might significantly distort the single-scattering signal whenever the scattering phase shifts are high (near $\pi/2$).

Fortunately for single-scattering contributions and for K-edge absorption $\chi_2^{ll'}=\chi_2^l \delta_{ll'}$,[24] so that these terms automatically drop out of the formula and the dipole-selection rule becomes again effective. However, for transitions from an L edge $\chi_2^{ll'}$ is not diagonal in l and we expect substantial deviations from this rule. It should be added, however, that in the usual experimental conditions the scattered electron beam is collected by a cylindrical mirror analyzer (CMA) that integrates over a spherical ring of 6° of aperture around its own axis. Due to the orthonormality of the spherical harmonics with respect to azimuthal integration, most of the off-diagonal terms cancel with the result that the validity of the dipole selection rule is approximately restored.

Although experimental evidence of such a dipole-selection rule has been reported by different experimental groups using different electron analyzers CMA,[9] Hemispherical analyzer,[10] and LEED analyzer,[4] this is the first time that it is shown to hold also for very deep edges which are generally more difficult to detect.

This paper is organized as follows. In Sec. II the experimental apparatus used for collecting the EELFS spectra above the Si K edge is described. Data structural analysis, following the usual EXAFS procedure, and the influence of the plasmon excitations by the primary incident beam, assessed through a deconvolution method, are presented in Sec. III. Finally, IV contains the general formulation of the electron energy-loss process in the reflection mode.

The distorted-wave Born approximation, used for such a formulation, allows us to incorporate in a manageable way both the full multiple scattering of the incident beam, before and after the collision and the complete multiple scattering of the excited electron of lower energy. Exchange process is taken into account in the way suggested by Saldin.[23]

EXPERIMENT

Silicon bars (111) were cleaved in UHV conditions and surface cleanliness was checked, before and after the EELFS measurements, by Auger analysis. The vacuum chamber was equipped with a Riber single-pass CMA with a coaxial electron gun.

Excitation beams with an energy of 3000 eV and current of 10 μA on 0.5 mm^2 were used. The EELFS measurements were carried out in the reflection mode at room temperature and at normal incidence of the primary beam.

10-V peak-to-peak modulation voltage was applied to the CMA to obtain the EELFS spectra. Signals were detected with a lock-in amplifier recording the first derivative of the electron yield distribution $dN(E)/dE$.

In these conditions the energy resolution $(\Delta E/E \sim 0.3\%)$ was about 5 eV. Data acquisition was performed with the help of an IBM computer interfaced with the lock-in amplifier. The collection time was about 60 min for each run.

It is well known that in the reflection mode the silicon energy-loss spectra show extended structures due to the plasmons replica. In order to assess their influence above the excited core edge these plasmons replica were collected close to the elastic peak with the same energy of the primary beam as used for the EELFS measurements. More details of the experimental apparatus have been reported elsewhere.[12]

RESULTS AND ANALYSIS

Figure 2 shows a typical EELFS result of the silicon K edge showing extended structure for about 300 eV beyond the edge located at 1840 eV. The EELFS oscillations obtained after subtraction of the smooth atomic background from the row data with the help of a cubic-spline procedure is shown in the lower part of Fig. 2.

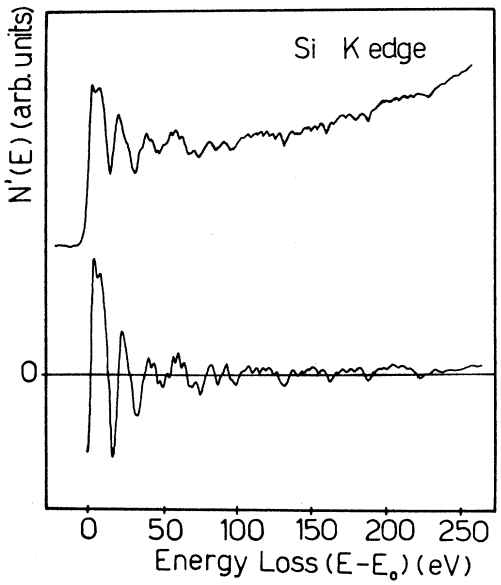

FIG. 2. Extended energy-loss fine structure above the K edge of the Si(111). The primary beam was $E_p=3$ keV. The spectrum is collected as the first derivative of the electron yield $N(E)$ and a modulation of 10 V was used. The lower part shows the extracted EELFS features after a smooth atomic background subtraction.

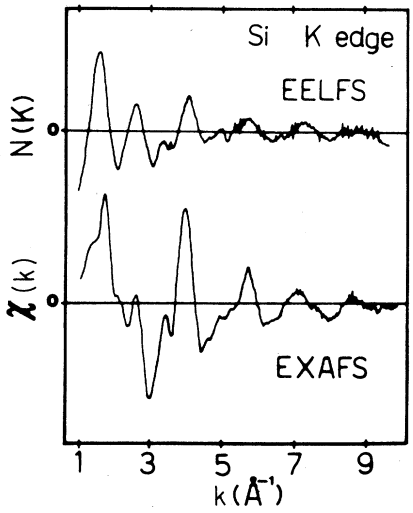

FIG. 3. Extended energy-loss fine structure above the K edge of the Si(111) clean surface. The spectrum, as a function of the k vector, has been obtained by numerical integration of the EELFS features displayed in Fig. 2. The lower part shows the EXAFS spectrum in the same K region for crystalline silicon as reported by Filliponi *et al.* (Ref. 17).

In order to compare directly our results with the EXAFS features, the original $dN(E)/dE$ EELFS spectra have been numerically integrated. The undifferentiated electron-energy-loss spectrum is shown in the upper part of Fig. 3 together with the EXAFS spectrum reported by Filipponi *et al.* (lower curve).[17] Both spectra are displayed as a function of the k wave vector given by

$$k(\text{Å}^{-1})=[0.263(E-E_0)(\text{eV})],^{1/2}$$

where E is the photon or loss energy, E_0 is the silicon K edge binding energy (1840 eV), and $(E-E_0)$ is the energy loss above the edge.

A strict analogy can be observed between the fine structure of the two spectra for what concerns the main frequency of the oscillating signal, apart from a slight difference in the low-k region. This discrepancy will be analyzed in terms of a convolution between electron single-scattering EELFS process and multiple plasmons excitation. The radial distribution function $F(R)$, which contains the structural information, has been obtained by Fourier-transform (FT) analysis of the integrated EELFS data.

This function, as shown in Fig. 4, displays several peaks as a function of the real-space distance R (Å) around the absorbing atom which should be related to the different neighbors in the crystalline Si arrangement. The main peak, at about 1.98 ± 0.03 Å, corresponds to the radius of the first atomic shell (2.35 Å).

This difference between our experimental lattice spacing and the crystallographic data, amounting to 0.37 Å, is attributed to the phase shift experienced by the excited electron involved in the EELFS process.[1] We note two other peaks located at 3.6 and 4.1 Å, respectively, which should correspond to the second and third nearest neighbors at 3.8 and 4.25 Å and to a double-scattering path at $R_{\text{tot}}=2\times4.27$ Å $=8.54$ Å.[18]

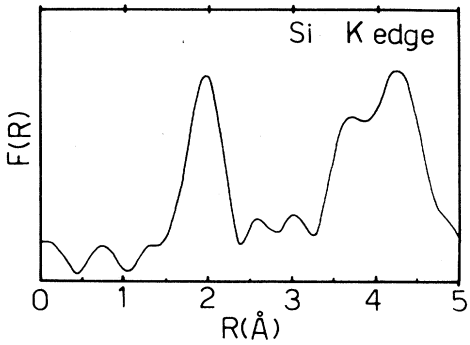

FIG. 4. Fourier transform of the EELFS data of Fig. 3. The different peaks, displayed as a function of the real space R(Å), correspond to the different neighbors of the silicon cage. The various features in the $F(R)$ are not corrected for the proper phase shift.

The intensity ratio of these two peaks to the first one does not agree with that reported by the different authors[17,19] in the EXAFS spectra. A possible origin of this discrepancy can be ascribed to the multiple plasmon contribution because the interaction between the impinging electron and the electronic system is particularly effective in exciting plasmons both before and after the absorption

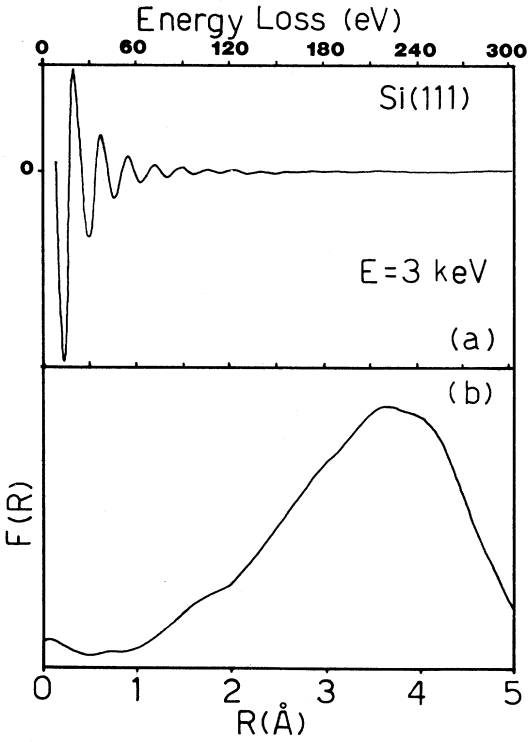

FIG. 5. (a) Plasmon features near the elastic peak for a Si(111) surface. We used the same 3-keV primary beam utilized for collecting the EELFS features. (b) Fourier transform of the above plasmonic features.

process.

Silicon moreover is a very good candidate for observing the multiple plasmon replica because its free-electron plasmon (located at ~17 eV) is not completely broadened by interband transitions as actually happens for the transitions metals where this multiple interaction is strongly screened.

In order to evaluate this contribution on the EELFS spectra we have measured the plasmon replica near the elastic peak using the same primary beam energy. The observed spectrum (upper curve) together with its Fourier transform (lower curve) is shown in Fig. 5 The FT of the plasmon replica spectrum has been performed in the same energy-loss range used for the EELFS FT analysis. In this way the broadening of the structure is comparable in both cases. The FT shown in Fig. 5(b) displays only a very broadened structure around 3.5 Å. In the Appendix we show that the observed core-edge spectrum $I_c(E)$ is the result of convolution of the single-scattering profile with a measured loss spectrum $I_l(E)$ close to the elastic peak as discussed by Leapman *et al.* for transmission energy-loss spectra:[25]

$$I_c(E)=I_s(E)*I_l(E) ,$$

where * denotes convolution. This single-scattering profile may be then recovered by deconvoluting the observed EELFS spectrum with the measured $I_c(E)$ spectrum using the following ratio:

$$\tilde{I}_s(E)=\tilde{I}_c(E)/\tilde{I}_l(E) ,$$

where ~ indicates the FT. The $F(R)$ resulting from this procedure is reported in Fig. 6(a). We note a lowering of the intensities of the second and third outer coordination shells which leads to a new ratio among the various structures. This deconvolution procedure gives now a more close correspondence between the $F(R)$ obtained by our EELFS data and that obtained by EXAFS analysis[17] reported in Fig. 6(b).

Since core excitations followed by multiple plasmon losses are possible, we have repeated the deconvolution process using a loss spectrum at a primary beam energy of 1 keV. We have found substantially, the same $F(R)$ as in Fig. 6(b). This is not surprising because of the saturation property of the extrinsic plasmon excitation process as described in Ref. 26.

It appears evident from the previous analysis that intensities (to a certain degree ±10%) and positions of the nearest neighbors are not affected by the presence of the multiple plasmons. This result allows us to extract the backscattering amplitude $\tilde{A}(k)$ and the phase shift $\phi(k)$ following the standard EXAFS procedure.[5,6] In Fig. 7 we show these extracted quantities as a function of the wave vector (solid line) together with the theoretical backscattering amplitude and phase shift reported by Teo and Lee[27] (dotted line) calculated in the dipole approximation ($s\rightarrow\epsilon p$ transitions). The two phase shifts are parallel over a wide k range suggesting the predominance of a single final-state l channel of the excited core electron.

Since the determination of the phase shift and in general all EXAFS analysis depend on the choice of the zero of energy for the photoelectron k vector, it is worthwhile

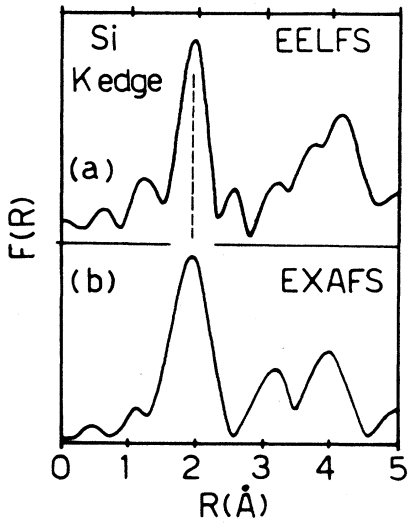

FIG. 6. (a) Fourier transform of the EELFS signal reported in Fig. 4 after deconvolution of the plasmon contribution shown in Fig. 5. The normalization procedure between the two FT functions is reported in the text. (b) Fourier transform of the EXAFS signal (Ref. 17) reported in Fig. 4.

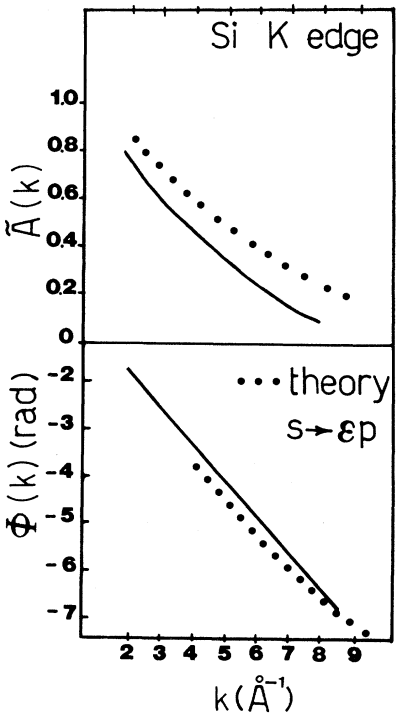

FIG. 7. Amplitude backscattering and phase shift obtained for the silicon K edge by means of the EXAFS procedure (Refs. 5 and 7) of the first nearest neighbors of the EELFS (FT) shown in Fig. 6(a) (solid line). The dotted lines represent the theoretical calculation of the same quantities reported by Teo and Lee (Ref. 27) for the silicon K edge.

spending a few words to illustrate our choice. In a muffin-tin model of the crystal, as the one usually used in this type of analysis, k is given by $k=(E-\mathbf{V}_0)^{1/2}$, where E is the kinetic energy of the photoelectron in vacuum (outside the system under study) and $\mathbf{V}_0$ is the average interstitial potential referred to the same vacuum. We have calculated $\mathbf{V}_0$ for a cluster of 17 Si atoms in tetrahedral coordination with touching atomic spheres and found $\mathbf{V}_0=-7$ eV. Since the work function for Si (top of valence band) is of the order of 5 eV taking into account a gap of ~ 1 eV gives zero of energy located ~ 2 eV below the rising edge (bottom of the conduction band). This is the definition we have adopted throughout our analysis, both theoretical and experimental, without making any adjustment.

THEORETICAL BACKGROUND

In discussing reflection electron-energy-loss fine-structure spectroscopy we must be aware that the Born approximation is usually not applicable, since for its validity the condition

$$\varepsilon_i(\varepsilon_s) \gg I$$

should be fulfilled both for the incident electron energy ε_i and for the scattered electron energy ε_s for excitation of a deep core state with ionization energy I. According to Mott and Massey[28] one should roughly have

$$\varepsilon_{i,s} \simeq 7I$$

which is clearly not the case for our experiment, in which $\varepsilon_i=3$ keV and $\varepsilon_s \simeq 1$ keV ($I \simeq 2$ keV). However in this latter case the distorted-wave Born approximation becomes applicable since, following Bethe and Jackiw,[29] the condition for the validity of the DWBA now becomes $\varepsilon_{i,s} > 250$ eV for any atom. For light atoms up to $Z=20$ the validity should start at a even lower energy.

In the distorted-wave scheme the differential cross section for inelastic scattering of an electron of initial energy $\varepsilon_i=k_i^2$ and wave vector $\mathbf{k}_i$ into a final state of energy $\varepsilon_s=k_s^2$ and wave vector $\mathbf{k}_s$, while the target system undergoes a transition from the initial ground state Ψ_0 of energy E_0 to a final state Ψ_n of energy E_n, is given by ($\Omega=\hat{\mathbf{k}}_s$)

$$\frac{d\sigma}{d\Omega}=\frac{1}{4\pi^2}\frac{k_s}{k_i}\sum_n |\langle \Psi_n \psi_s^- | V | \Psi_0 \psi_i^+ \rangle_d \pm \langle \psi_s^- \Psi_n | V | \Psi_0 \psi_i^+ \rangle_{\mathrm{ex}}|^2 \times \delta(E_0+\varepsilon_i-E_n-\varepsilon_s) , \tag{2}$$

where $\langle | V | \rangle_d$ is the direct Coulomb matrix element, $\langle | V | \rangle_{\mathrm{ex}}$ its exchange counterpart,[21,29] and the + sign is for triplet states; the − sign for singlet states.

We use atomic units throughout for lengths and Rydberg units for energies. For the direct matrix element in Eq. (2) we find

$$\langle \Psi_n \psi_s^- | V | \Psi_0 \psi_i^+ \rangle_d = \sum_{m=1}^{N} \int\int d\tau\, d^3r \frac{1}{|\mathbf{r}-\mathbf{r}_m|} \psi_i^+(\mathbf{r};\mathbf{k}_i)[\psi_s^-(\mathbf{r};\mathbf{k}_s)]^* \Psi_n(\mathbf{r}_1 \ldots \mathbf{r}_m \ldots \mathbf{r}_N)\Psi_0(\mathbf{r}_1 \ldots \mathbf{r}_m \ldots \mathbf{r}_N)$$
$$= \sum_{m=1}^{N} \int d\tau\, \Psi_n(\mathbf{r}_1 \ldots \mathbf{r}_m \ldots \mathbf{r}_N)\Psi_0(\mathbf{r}_1 \ldots \mathbf{r}_m \ldots \mathbf{r}_N) T_d(\mathbf{r}_m;\mathbf{k}_i,\mathbf{k}_s) , \tag{3}$$

where N is the total number of electrons in the target system, and

$$T_d(\mathbf{r}_m;\mathbf{k}_i\mathbf{k}_s)=\int d^3r \frac{1}{|\mathbf{r}-\mathbf{r}_m|}\psi_i^+(\mathbf{r},\mathbf{k}_i)[\psi_s^-(\mathbf{r};\mathbf{k}_s^-)]^* \tag{4}$$

is an effective transition operator. In these equations $\psi_i^+(\mathbf{r},\mathbf{k}_i)$ and $\psi_s^-(\mathbf{r},\mathbf{k}_s)$ are one-particle scattering states in the potential

$$u(\mathbf{r})=-\sum_{k=1}^{N/Z}\frac{2Z}{|\mathbf{r}-\mathbf{R}_k|}+\int\frac{\rho_0(\mathbf{r}')d^3r'}{|\mathbf{r}-\mathbf{r}'|} , \tag{5}$$

where R_k labels the position of the nuclei in the system, and

$$\rho_0(\mathbf{r})=\sum_{m=1}^{N}\int |\Psi_0(\mathbf{r}_1 \ldots \mathbf{r}_{m-1},\mathbf{r},\mathbf{r}_{m+1} \ldots \mathbf{r}_N)|^2 \times \prod_{j\neq m} d^3r_j .$$

(We have assumed that all nuclei in the system have the same atomic charge Z.) They behave asymptotically as

$$\psi_i^+(\mathbf{r},\mathbf{k}_i) \underset{r\to\infty}{\sim} e^{i\mathbf{k}_i\cdot\mathbf{r}}+f(\hat{\mathbf{k}}_i,\hat{\mathbf{k}}_i')\frac{e^{ik_ir}}{r} ,$$
$$\psi_s^-(\mathbf{r},\mathbf{k}_s) \underset{r\to\infty}{\sim} e^{i\mathbf{k}_s\cdot\mathbf{r}}+f^*(\hat{\mathbf{k}}_s,\hat{\mathbf{k}}_s')\frac{e^{-ik_sr}}{r} . \tag{6}$$

In a reflection EELFS experiment, these states are LEED states satisfying the conditions

$$\psi_i^+(\mathbf{r}+\mathbf{R}_m,\mathbf{k}_i)=e^{i\mathbf{k}_i\cdot\mathbf{R}_m}\psi_i^+(\mathbf{r},\mathbf{k}_i) ,$$
$$[\psi_s^-(\mathbf{r}+\mathbf{R}_m,\mathbf{k}_s)]^*=e^{-i\mathbf{k}_s\cdot\mathbf{R}_m}[\psi_s^-(\mathbf{r},\mathbf{k}_s)]^* , \tag{7}$$

where $\mathbf{R}_m$ are lattice vectors of the particular surface chosen. However since in our experimental conditions the penetration depth of the ingoing and outgoing electrons is large enough that we can consider the surface a small perturbation [at 1 keV this depth is several atomic layers ($\simeq 5-7$)] we can safely assume that in Eq. (7) $\mathbf{R}_m$

is the lattice vector of the entire crystal. The energy of 1 keV is somewhat a border line for an incident and scattered electron to be able to sample the full periodicity of the crystal. At somewhat lower energy ($\sim$20–600 eV) the periodicity of the sample along a direction perpendicular to the surface (z direction) cannot be sampled, since the electron mean free path drops down to $\sim$5 Å. However, the periodicity along the surface still holds true. In this case the full complication of LEED states should come into play.[30,31] The general treatment for this case will be given elsewhere,[32] although we can anticipate that the following conclusions still keep their validity. Using therefore the full periodicity of the system, we can find an alternative expression for the effective transition operator in Fig. 4. In fact, on the basis of Eq. (7) we can write for the quantity

$$\rho_{is}(\mathbf{r};\mathbf{k}_i,\mathbf{k}_s)=\psi_i^+(\mathbf{r},\mathbf{k}_i)[\psi_s^-(\mathbf{r},\mathbf{k}_s)]^* \tag{8}$$

the expansion

$$\rho_{is}(\mathbf{r},\mathbf{k}_i,\mathbf{k}_s)=\exp(i\mathbf{q}\cdot\mathbf{r})\sum_n \exp(i\mathbf{G}_n\cdot\mathbf{r})\rho(\mathbf{G}_n;\mathbf{k}_r,\mathbf{k}_s)\ , \tag{9}$$

where $\mathbf{q}=\mathbf{k}_i-\mathbf{k}_s$ is the momentum transfer and $\mathbf{G}_n$ are reciprocal lattice vectors of the crystal.

Substituting Eq. (9) into Eq. (4) and using the well-known formula

$$\int d^3r\frac{\exp(i\mathbf{q}\cdot\mathbf{r})}{r}=\frac{4\pi}{q^2}$$

one finds

$$T_d(\mathbf{r};\mathbf{k}_i,\mathbf{k}_s)=4\pi\sum_n \exp[i(\mathbf{q}+\mathbf{G}_n)\cdot\mathbf{r}]\frac{\rho(\mathbf{G}_n;\mathbf{k}_i,\mathbf{k}_s)}{|\mathbf{q}+\mathbf{G}_n|^2}\ . \tag{10}$$

The second matrix element in Eq. (2) is the exchange part given by

$$\langle\psi_s^-\Psi_n|V|\Psi_0\psi_i^+\rangle_{\rm ex}=\sum_{m=1}^{N}\int\int d\tau\,d^3r\frac{1}{|\mathbf{r}-\mathbf{r}_m|}\psi_i^+(\mathbf{r},\mathbf{k}_i)[\psi_s^-(\mathbf{r}_m,\mathbf{k}_s)]^*$$
$$\times\Psi_n(\mathbf{r}_1\ldots\mathbf{r}_{m-1}\ldots\mathbf{r}\ldots\mathbf{r}_{m+1}\ldots\mathbf{r}_N)\Psi_0(\mathbf{r}_1\ldots\mathbf{r}_m\ldots\mathbf{r}_N)\ .$$

To estimate this term, we use the asymptotic equation:[33]

$$\int\phi(\mathbf{r}')\frac{e^{i\mathbf{k}\cdot\mathbf{r}'}}{|\mathbf{r}-\mathbf{r}'|}d^3r'=\frac{4\pi}{k^2}e^{i\mathbf{k}\cdot\mathbf{r}}\phi(\mathbf{r})+O(k^{-3})\ ,$$

where $\phi(\mathbf{r})$ is a function which varies slowly compared with e^{ikr}. By writing

$$\psi_i^+(\mathbf{r};\mathbf{k}_i)=e^{i\mathbf{k}_i\cdot\mathbf{r}}\phi_i(\mathbf{r};\mathbf{k}_i)\ ,$$
$$\Psi_n(\mathbf{r}_1\ldots\mathbf{r}\ldots\mathbf{r}_n)=e^{i\mathbf{k}\cdot\mathbf{r}}\Phi_n(\mathbf{r}_1\ldots\mathbf{r}\ldots\mathbf{r}_n)\ ,$$

where $k=(\varepsilon_i+E_0-\varepsilon_s)^{1/2}=E_n^{1/2}$, in the hope that the product $\phi_i\phi_n$ be smooth on the scale of variation of $e^{i(\mathbf{k}_i-\mathbf{k})\cdot\mathbf{r}}$, we find

$$\langle\psi_s^-\Psi_n|V|\Psi_0\psi_i^+\rangle_{\rm ex}=\frac{4\pi}{|\mathbf{k}_i-\mathbf{k}|^2}\sum_{m=1}^{N}\int d\tau\,\psi_i^+(\mathbf{r}_m;\mathbf{k}_i)\psi_s^-(\mathbf{r}_m;\mathbf{k}_s)\Psi_n(\mathbf{r}_i\ldots\mathbf{r}_m\ldots\mathbf{r}_N)\Psi_0(\mathbf{r}_i\ldots\mathbf{r}_m\ldots\mathbf{r}_N)\ .$$

Remembering Eq. (9) we can finally write

$$M\equiv\langle\Psi_n\psi_s^-|V|\Psi_0\psi_i^+\rangle\langle\cdots\rangle_d+\langle\cdots\rangle\langle\psi_s^-\Psi_n|V|\Psi_0\psi_i^+\rangle_{\rm ex}$$
$$=\sum_{m=1}^{N}\int d\tau\,\Psi_n(\mathbf{r}_1\ldots\mathbf{r}_m\ldots\mathbf{r}_N)\Psi_0(\mathbf{r}_1\ldots\mathbf{r}_m\ldots\mathbf{r}_N)T(\mathbf{r}_m;\mathbf{k}_i,\mathbf{k}_s)\ , \tag{11}$$

where

$$T(\mathbf{r};\mathbf{k}_i\mathbf{k}_s)=4\pi\sum_n e^{i(\mathbf{q}_{Bz}+\mathbf{G}_n)\cdot\mathbf{r}}\left[\frac{1}{|\mathbf{q}_{Bz}+\mathbf{G}_n|^2}\pm\frac{1}{|\mathbf{k}_i-\mathbf{k}|^2}\right]\rho(\mathbf{G}_n;\mathbf{k}_i,\mathbf{k}_s) \tag{12}$$

is an effective transition operator containing both the direct and exchange contributions. Note that under the usual experimental conditions $|\mathbf{k}_i|\gg|\mathbf{k}|$.

In the determinantal approximation for the many electron states Ψ_0 and Ψ_n, Eq. (11) becomes

$$M=\sum_{m_0}\int_{V_0}d^3r\,\psi_{\mathbf{k}n}^*(\mathbf{r})T(\mathbf{r};\mathbf{k}_i\mathbf{k}_s)\phi_{L_0}^0(r)\ ,$$

where, in our case, $\phi_{L_0}^0$ is the wave function of the core electron with angular momentum $L_0\simeq(l_0,m_0)$ and $\psi_{\mathbf{k}n}$ that of the excitated electron with wave vector $\mathbf{k}$ relative to band n. We assume that $\phi_{L_0}^0(r)$ is normalized within the cell at site 0 of volume v_0.

The differential cross section Eq. (2) can then be written

$$\frac{d\sigma}{d\Omega}=\frac{1}{4\pi^2}\frac{k_s}{k_i}\sum_{kn}\sum_{m_0}|\langle\psi_{kn}|T|\phi^0_{L_0}\rangle|^2\delta(\varepsilon_0+\varepsilon_i-\varepsilon_{kn}-\varepsilon_s)$$

$$=-\frac{1}{4\pi^2}\frac{k_s}{k_i}\sum_{m_0}\frac{1}{\pi}\int\int_{v_0}\phi^0_{L_0}(\mathbf{r})T^*(\mathbf{r})\mathrm{Im}G(\mathbf{r},\mathbf{r}';\varepsilon)\times T(\mathbf{r}')\phi^0_{L_0}(\mathbf{r}')d^3r\,d^3r' , \tag{13}$$

where now ε_0 and ε_{kn} are one-particle energies such that $E_0-E_n=\varepsilon_0-\varepsilon_{kn}$ and $G(\mathbf{r},\mathbf{r}';\varepsilon)$ is the Green's function

$$G(\mathbf{r},\mathbf{r}';\varepsilon)=\sum_{kn}\frac{\psi^*_{\mathbf{k}n}(\mathbf{r})\psi_{kn}(\mathbf{r}')}{\varepsilon-\varepsilon_{\mathbf{k}n}} \tag{14}$$

with $\varepsilon=\varepsilon_0+\varepsilon_i-\varepsilon_s$. The functions $\psi_{\mathbf{k}n}(\mathbf{r})$ are Bloch function of the crystal with energies $\varepsilon_{\mathbf{k}n}$, n labeling the band and $\mathbf{k}$ being the Brillouin-zone vector. They obey the Schrödinger equation

$$[\nabla^2+\varepsilon_{\mathbf{k}n}-V(\mathbf{r})]\psi_{kn}(\mathbf{r})=0 , \tag{15}$$

where $V(\mathbf{r})$ is the self-consistent periodic crystal potential. It is well known and can be easily verified from Eq. (14) and (15) that $G(\mathbf{r},\mathbf{r}';\varepsilon)$ satisfies the equation

$$[\nabla^2+\varepsilon-V(\mathbf{r})]G(\mathbf{r},\mathbf{r}';\varepsilon)=\delta(\mathbf{r}-\mathbf{r}') \tag{16}$$

with periodic conditions

$$G(\mathbf{r}+\mathbf{R}_m,\mathbf{r}'+\mathbf{R}_m;\varepsilon)=G(\mathbf{r},\mathbf{r}';\varepsilon) \tag{17}$$

due to Eq. (14) and the property of Bloch states

$$\psi_{\mathbf{k}n}(\mathbf{r}+\mathbf{R}_m)=e^{i\mathbf{k}\cdot\mathbf{R}_m}\psi_{\mathbf{k}n}(\mathbf{r}) .$$

Zeller[34] has shown that a direct space solution of Eq. (16) with periodicity conditions given by Eq. (17) is provided by the expression

$$G(\mathbf{r}_m+\mathbf{R}_m,\mathbf{r}'_n+\mathbf{R}_n;\varepsilon)=\delta_{mn}G^m_s(\mathbf{r}_m,\mathbf{r}'_n;\varepsilon)-k\sum_{LL'}R^m_L(\mathbf{r}_m)\tau^{mn}_{LL'}R^n_{L'}(\mathbf{r}'_n) , \tag{18}$$

where $k=(\varepsilon)^{1/2}$ and $\mathbf{r}_n=\mathbf{r}-\mathbf{R}_m$, so that $\mathbf{r}_m$ and $\mathbf{r}'_n$ are confined to unit cells m and n, respectively. In the muffin-tin (MT) approximation, the function $R_L(\mathbf{r})$ can be written as

$$R_L(\mathbf{r})=R_l(r)Y_L(\hat{\mathbf{r}}) , \tag{19}$$

where $R_l(r)$ is that solution of the radial Schrödinger equation regular at the origin, that matches smoothly to

$$j_l(kr)\mathrm{cotan}\delta_l-n_l(kr) \tag{20}$$

at the MT sphere radius. Here δ_l is the lth phase shift of the MT sphere potential, in terms of which the atomic t_l matrix is given by $t_l=\exp(i\delta_l)\sin\delta_l$. The quantity $\tau^{mn}_{LL'}$ is the scattering path operator given by

$$\tau^{mn}_{LL'}=(M^{-1})^{mn}_{LL'} ,$$

where

$$M^{mn}_{LL'}=(t^m_l)^{-1}\delta_{mn}\delta_{LL'}+G^{mn}_{LL'}(1-\delta_{mn}) \tag{21}$$

is the multiple-scattering matrix and $G^{mn}_{LL'}$ is the spherical-wave propagator given by

$$G^{mn}_{LL'}=-4\pi i\sum_{L''}i^{l-l'+l''}C^{L'}_{LL''}h^+_{l''}(\mathbf{k}\cdot\mathbf{R}_{mn})Y_{L''}(\hat{\mathbf{R}}_{mn}) \tag{22}$$

with

$$C^{L'}_{LL''}=\int d\Omega\, Y_L(\Omega)Y_{L'}(\Omega)Y_{L''}(\Omega) ,$$

$$\mathbf{R}_{mn}=\mathbf{R}_m-\mathbf{R}_n$$

h^+_l being the Hankel function and using real-spherical harmonics. Assuming for simplicity that there is only one atom for unit cell, the index m on t^m_l can be omitted. The generalization to more atoms per unit cell is straightforward. Note that, because of the periodicity $\tau^{mn}_{LL'}$ depends only on $\mathbf{R}_{mn}$.

In terms of Eqs. (19) and (20) the single cell Green's function $G^m_s(\mathbf{r},\mathbf{r}')$ is given by

$$G^m_s(\mathbf{r}_m,\mathbf{r}'_m)=k\sum_{LL'}R_L(\mathbf{r}_m)\tau^{mm}_{LL'}R_{L'}(\mathbf{r}'_m)-k\sum_L R_L(\mathbf{r}_m)S_L(\mathbf{r}'_m) , \tag{23}$$

where $S_L(\mathbf{r})=S_l(r)Y_L(\hat{\mathbf{r}})$ and $S_l(r)$ is that solution of the radial Schrödinger equation, singular at the origin, that matches smoothly to $j_l(kr)$ at the MT sphere radius. As shown by Zeller,[34] the solution given by Eqs. (19) and (20) is not restricted to MT potentials. With a different prescription for $R_L(r)$ and $S_L(r)$, it can be proved to hold in the case of general potentials. Also, if this latter is real, $R_L(r)$ and $S_L(r)$ can be shown to be real. Therefore we can write in all generality

$$\mathrm{Im}G(\mathbf{r},\mathbf{r}';\varepsilon)=-k\sum_{mn}\sum_{LL'}R_L(\mathbf{r}_m)(\mathrm{Im}\tau^{mn}_{LL'})R_{L'}(\mathbf{r}_n) \tag{24}$$

and clearly

$$\mathrm{Im}G(\mathbf{r}+\mathbf{R}_{m'},\mathbf{r}'+\mathbf{R}_m;\varepsilon)=\mathrm{Im}G(\mathbf{r},\mathbf{r}';\varepsilon) . \tag{25}$$

Due to the localization of the initial state core wave function, we actually need $G(\mathbf{r},\mathbf{r}')$ for $\mathbf{r}$ and $\mathbf{r}'$ inside cell at site 0. Consequently Eq. (12) becomes

$$\frac{d\sigma}{d\Omega}=\frac{1}{4\pi^2}\frac{k_s}{k_i}\frac{k}{\pi}\times\sum_{m_0}\sum_{LL'}\int\int_{v_0}\phi^0_{L_0}(\mathbf{r}_0)T^*(\mathbf{r}_0;\mathbf{k}_i\mathbf{k}_s)R_L(r_0)\mathrm{Im}\tau^{00}_{LL'}\times R_{L'}(\mathbf{r}_0)T(\mathbf{r}'_0;\mathbf{k}_i\mathbf{k}_s)\times\phi^0_{L_0}(\mathbf{r}'_0)d^3r_0\,d^3r'_0 . \tag{26}$$

Two consequences can be read out from this equation and Eq. (12) for the transition operator. The first one is that the total momentum transfer is given by $\mathbf{q}=\mathbf{k}_i-\mathbf{k}_s$ plus any reciprocal lattice vector $\mathbf{G}_n$, including $\mathbf{G}_n=0$. When $\mathbf{G}_n\neq0$ this observation substantiates the common picture of the reflection energy-loss process as composed of two independent steps: diffraction of the incident vector $\mathbf{k}_i$ and subsequent energy loss or energy loss followed

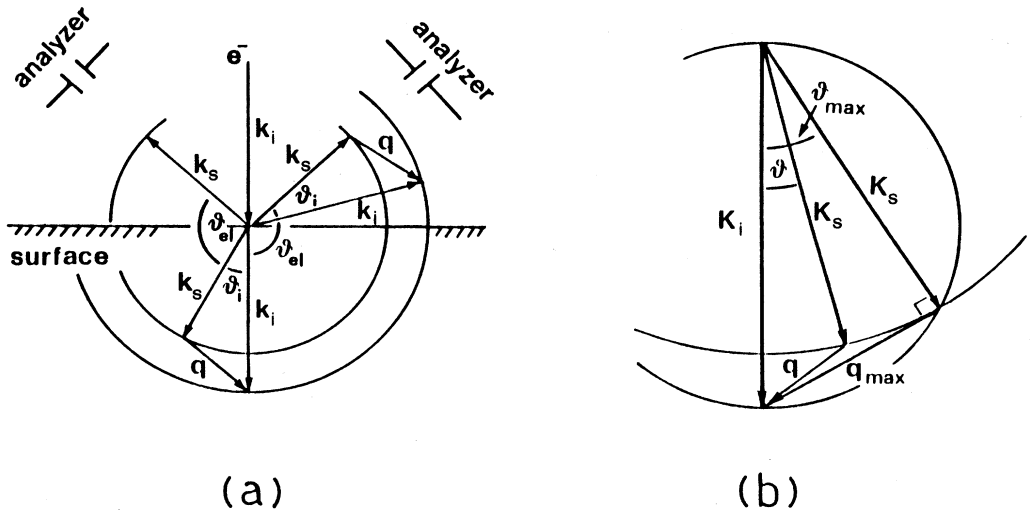

FIG. 8. (a) k vector diagrams showing reflection energy-loss processes. The inelastic scattering detected in the electron analyzer can be analyzed in terms of a two-step process: an inelastic scattering event at θ_i, followed or preceded by an inelastic backscattering with θ_{el}. The elastic diffraction before loss (DL) and loss before elastic diffraction (LD) have a greater probability to occur compared to the two other processes involving a direct backscattering and a double backscattering as reported by Froitzheim (Ref. 35). (b) Schematic vector diagram of inelastic scattering process in a DL and LD mechanism. k_i is the momentum of the incoming electron, k_s is the momentum of the scattered electorn, and q is the momentum transferred. For a given loss ΔE the transferred momentum q may vary from a minimum value given by $q_{\min}(\text{Å}^{-1})=(0.263E_p)^{1/2}-[0.263(E_p-\Delta E)]^{1/2}$ to a maximum value given by $q_{\max}=(0.263\Delta E)^{1/2}$ following the argument given in the text (Refs. 35–37). In a DL or LD process the maximum value of the diffusion angle $\theta_{\max}$ may be $\pi/2$ when $\Delta E=E_p$.

by diffraction of the scattered vector $\mathbf{k}_s$ as discussed by Froitzheim,[35] Avery[36] and Nassiopulos and Cazaux.[37] These two processes are schematically depicted in Fig. 8(a).[37] It is to be noted, however, that the two-step process does not necessarily imply "small" momentum transfer and small-angle scattering. As discussed later on the scattering angles can be as large as $\pi/2$. When $\mathbf{G}_n=0$, we speak of one-step processes, in which the crystal does not intervene in the deflection of the primary beam.

The second one concerns the structural information embodied in $\tau^{00}_{LL'}$. Apart from questions of selection rules, which we shall discuss in a moment, this is exactly the same quantity which is measured in a photoabsorption experiment. As is well known, in the MT approximation, and for polarization averaged cross section,[38]

$$\chi^l(k)=\frac{1}{\sin^2\delta^0_l}\frac{1}{2l+1}\mathrm{Im}\sum_m \tau^{00}_{lm,lm}=1+\sum_{n=2}^{\infty}\chi^l_n(k)\ , \tag{27}$$

where $\chi^l_n(k)$ is the contribution of the nth order multiple-scattering (MS) paths beginning and ending at site 0, for a final l state. In particular $\chi^l_2(k)$ is the usual EXAFS signal. Equation (27) is obviously meaningful if the MS series on the right-hand side converges. Apart from prefactors, the expression (26) has the same structure as for a photoabsorption process. The only differences lie in the transition operator $T(\mathbf{r})$. Whereas with photons the dipole operator is effective in selecting only two final L channels, in principle such a selection is not effective in a EEL process.

Since, from Eq. (12) $T(\mathbf{r};\mathbf{k}_i,\mathbf{k}_s)$ is a linear combination of plane waves with wave vector $\mathbf{q}_n=\mathbf{q}+\mathbf{G}_n$, for which the angular-momentum development is

$$e^{i\mathbf{q}_n\cdot\mathbf{r}}=4\pi\sum_L i^l j_l(q_n r)Y_L(\hat{\mathbf{r}})Y_L(\hat{\mathbf{q}}_n)\ ,$$

by defining

$$M^{l_0}_{l_t l}(q_n)=\int_0^{r_s} r^2 dr\ \phi^0_{l_0}(r)j_{l_t}(q_n r)R_l(r)\ , \tag{28}$$

where r_s is the MT sphere radius, we obtain

$$\begin{aligned}M_{L_0L}&=\int_{v_0}\phi^0_{L_0}(\mathbf{r})T^*(\mathbf{r};\mathbf{k}_i\mathbf{k}_s)R_L(\mathbf{r})d^3r\\&=\sum_{L_t}\sum_n 16\pi^2\left[\frac{1}{q_n^2}\pm\frac{1}{|\mathbf{k}_i-\mathbf{k}|^2}\right]\rho^*(\mathbf{G}_n,\mathbf{k}_i,\mathbf{k}_s)\\&\quad\times i^{-l_t}M^{l_0}_{l_0 l}(q_n)C^{L_0}_{L_t L}Y_{L_t}(\hat{\mathbf{q}}_n)\ .\end{aligned} \tag{29}$$

This expression simplifies further if we specialize to $L_0=0$, as for our experiment. Then, since $C^0_{L_t L}=\delta_{L_t L}1/(4\pi)^{1/2}$ we find

$$M_L \equiv M_{0L} = \sum_n \frac{4\pi}{q_n^2}\left[1 \pm \frac{q_n^2}{|\mathbf{k}_i - \mathbf{k}|^2}\right](4\pi)^{1/2}\rho^*(\mathbf{G}_n;\mathbf{k}_i,\mathbf{k}_s) \times i^{-l} M_l^0(q_n) Y_L(\hat{\mathbf{q}}_n) = \sum_n \frac{4\pi}{q_n^2} A_n^*(q_n;\mathbf{G}_n) M_l^0(q_n) Y_L(\hat{\mathbf{q}}_n) , \quad (30)$$

where

$$M_l^0(q_n) = \int_0^{r_s} \phi_0^0(r) j_l(q_n r) R_l(r) r^2 dr \quad (31)$$

and

$$A_n(q_n;\mathbf{G}_n) = \left[1 \pm \frac{q_n^2}{|\mathbf{k}_i - \mathbf{k}|^2}\right](4\pi)^{1/2}\rho(\mathbf{G}_n;\mathbf{k}_i,\mathbf{k}_s) i^{-l} . \quad (31a)$$

For a K-edge excitation we then find

$$\frac{d\sigma}{d\Omega} = \frac{1}{4\pi^2}\frac{k_s}{k_i}\frac{k}{\pi}\sum_{LL'} M_L^* \mathrm{Im}\tau_{LL'}^{00} M_{L'} = 4\frac{k_s}{k_i}\frac{k}{\pi}\sum_{nn'}\sum_{LL'} \frac{A_n^*(q_n;\mathbf{G}_n)}{q_n^2}\frac{A_{n'}(q_{n'};\mathbf{G}_{n'})}{q_{n'}^2} M_l(q_n) Y_L(\hat{\mathbf{q}}_n) \mathrm{Im}\tau_{LL'}^{00} M_{l'}(q_{n'}) Y_{L'}(\hat{\mathbf{q}}_{n'}) . \quad (32)$$

Due to the interference effects we expect that only the diagonal terms in this sum contribute to the measured signal, especially if many n and L terms contribute. Moreover, since

$$\mathbf{q}_n = \mathbf{k}_i - \mathbf{k}_s + \mathbf{G}_n$$

we find

$$q_n^2 = k_i^2|\mathbf{k}_s - \mathbf{G}_n|^2 - 2k_i|\mathbf{k}_s - \mathbf{G}_n|\cos\theta_n ,$$

where θ_n is the angle between $\mathbf{k}_i$ and $\mathbf{k}_s - \mathbf{G}_n$. Thence

$$q_n dq_n = |\mathbf{k}_s - \mathbf{G}_n| k_i \sin\theta_n d\theta_n .$$

Therefore, taking into account that in the diffraction process the modulus of $\mathbf{k}_s$ is conserved ($|\mathbf{k}_s - \mathbf{G}_n| = |\mathbf{k}_s|$) and integrating over the acceptance of the CMA analyzer, what is measured is

$$\sigma_{\mathrm{ac}} = \frac{8\pi}{k_i^2}\sum_n\sum_L \int_{q_{\min}}^{q_{\max}} q_n dq_n \frac{|A_n(q_n;\mathbf{G}_n)|^2}{q_n^4}[M_l^0(q_n)]^2 \frac{k}{\pi}\mathrm{Im}\tau_{LL}^{00}\frac{1}{2\pi}\int_0^{2\pi} d\phi_n Y_L^2(\hat{\mathbf{q}}_n) + \text{background}$$
$$= \frac{8\pi}{k_i^2}\sum_n\sum_L \int_{q_{\min}}^{q_{\max}} dq_n \frac{|A_n(q_n;\mathbf{G}_n)|^2}{q_n^3}(2l+1)[\tilde{M}_l^0(q_n)]^2\left[1 + \sum_{\nu=2}^{\infty}\chi_\nu^l(k)\right] \times \frac{1}{2\pi}\int_0^{2\pi} d\phi_n Y_L^2(\hat{\mathbf{q}}_n)\frac{1}{2l+1} + \text{background} . \quad (33)$$

Remembering the definition (27) and introducing the atomic matrix element

$$\tilde{M}_l^0(q_n) = \left[\frac{k}{\pi}\right]^{1/2} \sin\delta_l^0 M_l^0(q_n) . \quad (34)$$

In Eq. (33) $q_{\min}$ is given by

$$q_{\min} = k_i - k_s ,$$

whereas for $q_{\max}$ values up to

$$q_{\max} = k_i + k_s$$

would be possible. In practice, following the argument given in Ref. 29 (p. 301), the EEL cross section is not negligible only for $q = \bar{q}_{\max} \ll q_{\max}$, where $\bar{q}_{\max}$ is an effective $q_{\max}$. To find out this effective $\bar{q}_{\max}$ one observes that $\bar{q}_{\max} r_c \gg 1$, where r_c is the radius of the initial core state. Therefore the integral

$$\int \phi_{L_0}^0(\mathbf{r})\exp(-i\mathbf{q}_n\cdot\mathbf{r})R_L(\mathbf{r})$$

occurring into Eq. (26) for the cross section is sizable only if the continuum wave function $R_L(\mathbf{r})$ varies as $\exp(-i\mathbf{q}_n\cdot\mathbf{r})$ i.e., if the final state of the excited atomic electron has momentum $\mathbf{q}_n$. This implies that there is approximate momentum conservation between the incident electron and the excited electron. Therefore

$$\bar{q}_{\max} \simeq (\Delta\varepsilon)^{1/2} \simeq (k_i^2 - k_s^2)^{1/2} .$$

Inserting this into the relation

$$q_i^2 = k_i^2 + k_s^2 - 2k_i k_s\cos\theta_i$$

for a single inelastic process without diffraction, one obtains for θ_i the limits $0 \le \theta_i \le \theta_i(\max)$ with $\theta_i(\max) = \sin^{-1}(\Delta\varepsilon/\varepsilon_i)^{1/2}$ and the maximum of $\theta_i(\max)$ is $\pi/2$, which is reached when $\Delta\varepsilon = \varepsilon_i$ [see Fig. 8(b)]. Therefore we must conclude that most of the inelastic events occur in a "forward" half-space, i.e., in that region of space limited by the crystal surface and lying on the side of the positive $\mathbf{k}_i$ direction (crystal bulk). Since the final $\mathbf{k}_s$ direction points in the opposite half-space, this means that the energy losses observed during reflection from surfaces are accompanied by elastic collision, as already noted by several authors.[35–37] To this effect the sum over n in Eq. (33) is over those $\mathbf{G}_n$ which transfer $\mathbf{k}_s$ into the acceptance of the CMA. This restriction rules out one-step momentum transfer as being significant in

the loss process, both because of matrix elements order of magnitude arguments and because of the depressing factor $1/q^3$.

We have easily adapted a multiple-scattering program to calculate the radial wave function $R_l(r)$ in a muffin-tin potential for silicon constructed according the usual Mattheis prescription.[39] The results are presented in Fig. 9 and show a substantial predominance of the $l=1$ component of the quantity

$$S(q_n)\equiv\frac{8\pi}{k_i^2}(2l+1)|\tilde{M}_l^0(q_n)|^2 \tag{35}$$

expressed in kilobarns (10^{-21} cm^2).

This predominance is greatly enhanced by the fact that actually what is observed, according to Eq. (33), is the integral of the function $S(q_n)/q^3$ which is reported in Fig. 10, in units of 10^{-32} cm^3. This figure shows that the $l=1$ component substantially accounts for the integrated cross section σ_{ac} in the whole q_n range between q_{min} and q_{max}. This conclusion is reinforced by the fact that $|A_n(q_n;\mathbf{G}_n)|^2$ decreases with increasing q_n.

From Figs. 9 and 10 we see that in practice only the monopole and the dipole transitions are sizable. This is a consequence of the behavior of $j_l(qr)$ in the matrix element (31). In fact since

$$\rho^2 j_l(\rho)\sim\rho^{2+l}/(2l+1)!!$$

for $\rho<l$ and qr varies between $q_{min}r_c\sim 6(\frac{3}{2})(1/Z)=9/Z$ and $q_{max}r_c\sim 10(\frac{3}{2})(1/Z)=15/Z$, where $r_c=\frac{3}{2}(1/Z)$ is the radius of the core state, only the $l=0$ and $l=1$ matrix elements in Eq. (31) turn out to be non-negligible ($Z=14$ for Si).

In this case interference effects in the various L channels are no more operative and Eq. (33) should be replaced by

$$\sigma_{ac}=\frac{8\pi}{k_i^2}\sum_n\sum_{ll'}^{1}\int_{q_{min}}^{q_{max}}dq_n\frac{|A_n(q_n;\mathbf{G}_n)|^2}{q_n^3}\times N_{ll'}\tilde{M}_l^0(q_n)\tilde{M}_{l'}^0(q_n)\frac{1}{2\pi}\times\int_0^{2\pi}d\phi_n\chi^{ll'}(k,\hat{\mathbf{q}}_n)\,, \tag{36}$$

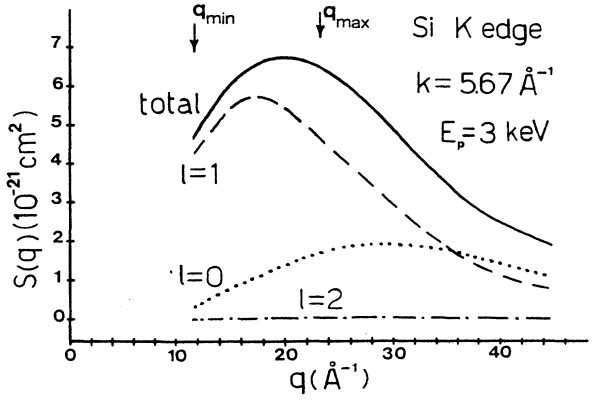

FIG. 9. Plot of the quantity $S(q)$ [Eq. (35) of the text] for the various l components contributing to the electron scattering cross section. Units are in kilobarns (10^{-21} cm^2).

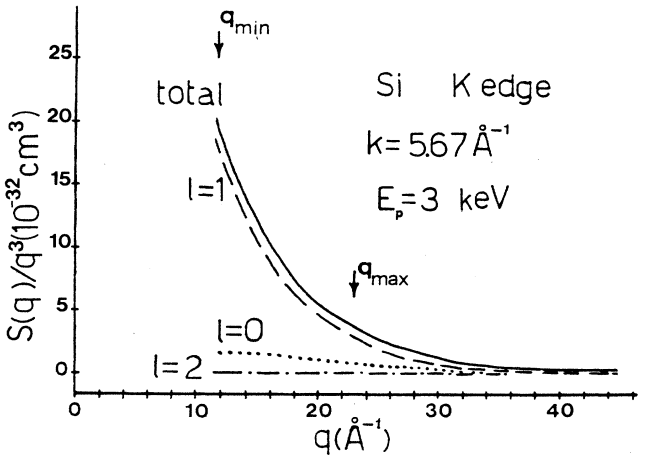

FIG. 10. Plot of the quantity $S(q)/q^3$ expressed in units of 10^{-32} cm^3. Upon multiplication with q_n (in cm^{-1}) one would obtain an average value, in cm^2, of the electron scattering cross section.

where now

$$\chi^{ll'}(k,\hat{\mathbf{q}}_n)=\frac{1}{N_{ll'}}\frac{1}{\sin\delta_l^0}\frac{1}{\sin\delta_{l'}^0}\times\sum_{mm'}\mathrm{Im}\tau_{lm,l'm'}^{00}Y_{lm}(\hat{\mathbf{q}}_n)Y_{l'm'}(\hat{\mathbf{q}}_n)$$
$$=1+\sum_{v=2}^{\infty}\chi_v^{ll'}(k,\hat{\mathbf{q}}_n)$$

and $N_{ll'}$ is an appropriate normalization factor.[24,38]

Fortunately enough, as anticipated in the Introduction, the main single-scattering signal $\chi_2^{ll'}(k,\hat{\mathbf{q}}_n)$ is diagonal in l for the K-edge absorption.[24] Moreover the azimuthal integration eliminates the off-diagonal terms in m, so that $M_0^0(q_n)M_1^0(q_n)$ is only 25% of $[M_1^0(q_n)]^2(2l+1)$ even for the higher-order multiple-scattering terms.

The above result supports the claim that one can analyze EELFS as if the dipole selection rule was effective, even in reflection mode and at relatively low incident and scattered energies, at least for initial nodeless core states.

Note that in our experiment conditions $k_i^2=3$ keV, $k_s^2=1.2\simeq 1$ keV, and the energy loss $\Delta\varepsilon=1.8\simeq 2$ keV. At the silicon K edge $q_{min}=k_s-k_i=6$ a.u.$^{-1}$ and r_c, the radius of the core state, is $r_c=\frac{3}{2}1/Z=\frac{3}{28}\simeq\frac{1}{9}$ a.u., so that $q_{min}r_c\simeq\frac{6}{9}=\frac{2}{3}$. Therefore, already at the minimum momentum transfers, the condition for the validity of the dipole approximation ($qr\ll 1$) is violated. Moreover many other momentum transfer q_n, such that $q_nr_c\gg 1$, intervene in the expression (12) for the transition operator, since the condition $\Delta E/E_0\ll 2(R)^{1/2}$, where $R(\simeq 10^{-2})$ is a LEED reflection matrix, is not satisfied in our case ($\Delta E/E_0=\frac{2}{3}$). This condition would in fact insure the predominance of the small-angle scattering events followed or preceded by an elastic diffraction as pointed out by Saldin.[23] Therefore the predominance of the $l=1$ component in the total cross section was to be ascertained in the whole range of variation of $\mathbf{q}_n$.

To obtain further evidence that the dipole component is the dominant signal we have calculated the unpolarized

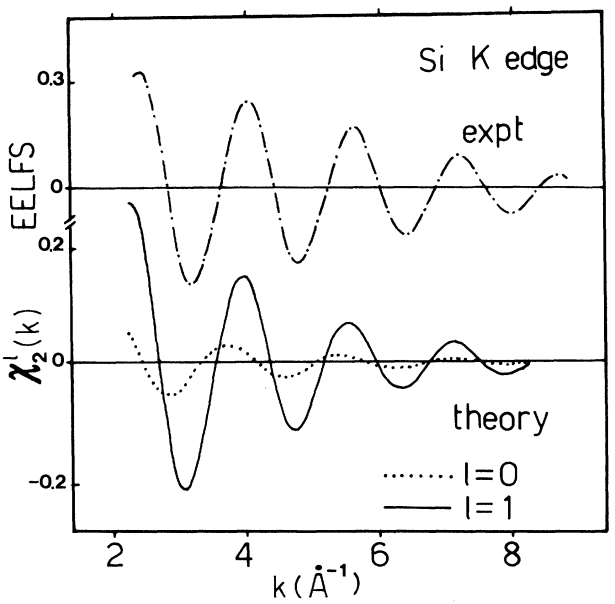

FIG. 11. Comparison between the experimental EELFS oscillation obtained by back-Fourier transform of the first peak of the $F(R)$ of Fig. 4 and theoretical calculation of unpolarized EXAFS signal for the first coordination shell for $l=0$ and $l=1$ final states, according to Eq. (37). The weight of the atomic matrix elements for monopole and dipole terms has been considered as shown in Fig. 9.

EXAFS oscillation $\chi_2^l(k)$ for the first coordination shell of Si (Ref. 18) and for $l=0$ and $l=1$ final states. The comparison shown in Fig. 11 with the back-Fourier transform of the first peak in Fig. 4, shows an excellent phase agreement with the $l=1$ component, whereas the monopole transition ($l=0$) is slightly out of phase particularly at low-k values.

The theoretical $\chi_2^l(k)$ signal has been calculated using the curved wave formula[38] with the usual Debye-Waller factor to take into account thermal disorder. The phase shift have been computed with the Mattheis prescription[39] for the potential and the $X-\alpha$ approximation for exchange and correlation part.

Furthermore the amplitude of the $\chi_2^{l=0}(k)$ signal has been reduced by the ratio $[M_0^0(q_n)]^2/\{(2l+1)[M_1^0(q_n)]^2\}\simeq\frac{1}{6}$ derived from Fig. 9 when q_n is about $(q_{\max}+q_{\min})/2$.

CONCLUSIONS

By a careful comparison between reflection EELFS and EXAFS spectra of the same compound, we have shown that reliable structural information can be obtained also with electron. Since spectra can be collected in any UHV system, this technique represents a complementary tool to other electronic spectroscopies, like Auger, x-ray photoemission spectroscopy, and EELS.

The main objective of this work was to determine whether an approximate dipole selection rule is effective in a reflection electron-energy-loss experiment for excitation of a deep core electron when the energy of the primary beam is comparable with the core ionization energy. Both on the basis of experimental and theoretical analysis we have shown that an effective dipole selection rule is at work even in this latter case.

On the experimental side, the good agreement between the FT of the EELFS and the EXAFS signal provides evidence that the structural information is the same on both spectroscopies, after correction for plasmon losses in the electron case.

On the theoretical side, although we have used the DWBA for calculating the electron scattering cross section, we have been able to reduce the analysis to the simpler Born approximation, by expanding the LEED states of the incoming and outgoing electron in their plane-wave components.[23] The resulting cross section then appears as an interference process between all possible amplitudes for the exciting electron to undergo diffraction before loss or loss before diffraction and for the *excited* electron to travel any MS closed path, standing at the site of the excited atom with angular momentum L and returning to the same site with angular momentum L'.

Due to the behavior of $r^2 j_l(q_r)$ in Eq. (31), only the $l=0$ and $l=1$ final-state channels turn out to be non negligible, the monopole transition being depressed by the factor 5–10 with the respect to the dipole transition. The depressing mechanism for the $l=0$ channel is due to the fact that in the radial matrix element

$$M_l^0(q)=\int_0^\infty \phi_0^0(r) j_0(qr) R_0(r) r^2 dr$$

one can neglect in a first approximation $j_0(qr)=\sin(qr)/qr\sim 1$ for $qr<1$. Consequently $M_l^0(q)=0$, due to the orthogonality of $\phi_0^0(r)$ and $R_0(r)$, since they are eigenstates of the same Hamiltonian (if relaxation effects are taken into account, the continuum wave function should be made orthogonal to the initial state to satisfy the Pauli principle). In practice, due to the slight variation of $j_0(qr)$ with r, a small contribution comes also from the $l=0$ channel. A further evidence of this predominance comes from the comparison of the back-Fourier (BF) transform of the first shell around of the excited atom with the unpolarized $\chi_2^l(k)(l=0,1)$ signal calculated for the same shell. The dipolar signal ($l=1$) is in phase with the BF oscillation, whereas the monopole signal is slightly out of phase.

For transition from deep core state this approach seems to be preferable to that of Ref. 22 since the convergence in l is faster and therefore the multipolar analysis simpler. Finally the contribution of cross-channel transitions has been shown to be depressed by the averaging over the azimuthal angle performed by the CMA analyzer.

It is worth remembering that the above conclusions hold for transitions from a nodeless, well-localized core state. Their validity for other initial states should be verified by explicit calculations. It is in fact difficult to generalize the argument about the ratio of the various l channels to transitions from general initial core states of the principle quantum number n_0 and angular momentum l_0. In this case the relevant matrix element is given

by Eq. (28) with the constraint $|l_0-l_f|\le l\le|l_0+l_f|$. The size of this integral clearly depends on the extension of the core state, the relative position of the nodes of the integrand functions and it is almost impossible to draw general conclusions for any type of initial state. For nodeless localized states phenomena like Cooper minima are ruled out, and it is safer to draw general conclusions.

APPENDIX

We discuss here in more detail the assumptions underlying the procedure to extract the single-scattering signal $I_s(\Delta E)$ from the observed electron-energy-loss spectrum $I_c(\Delta E)$, where $\Delta E=E_i-E_s$ is the energy loss. Since we want to assess the influence of the energy dependence of the atomic ionization cross section and the effect of averaging over a finite solid angle (the acceptance of the CMA analyzer) on the convolution procedure used in Sec. III, we introduce a differential scattering signal $I_s(\Delta E,q_n)$ choosing as an independent variable the momentum transfer q_n rather than the scattering angles θ and ϕ. Of the three independent variables needed to characterize the vector $\mathbf{q}_n$, we shall assume that $\mathbf{q}_n=\mathbf{q}$ and $\phi_q=\phi$ are really independent, whereas θ_q, the polar angle of $\mathbf{q}_n$ with respect the direction of k_i, will be considered a function of q_n through the relation

$$q^2=-\Delta E+2\sqrt{E_i}q\cos\theta_q \tag{A1}$$

which is derived by applying the Carnot theorem to the vector relation $\mathbf{q}=\mathbf{k}_i-\mathbf{k}_s-\mathbf{G}_n$ and using $|\mathbf{k}_s-\mathbf{G}_n|=k_s$.

On the basis of Eq. (36) of the text we can write schematically

$$I_s(\Delta E,\mathbf{q}_n)=\chi(\Delta E,\hat{\mathbf{q}}_n)\frac{F(q)}{E_i}\ , \tag{A2}$$

where $F(q)/E_i$ is a smooth atomic differential cross section and $\chi(\Delta E,\hat{\mathbf{q}}_n)$ is the fine-structure signal, depending only on the polar angles θ_q and ϕ. For simplicity we have dropped the sums over l,l',n appearing in Eq. (36) which can be restored when needed. The integrated cross section over the acceptance of the CMA is therefore given by

$$\begin{aligned}\langle I_s(\Delta E,E_i)\rangle_{\rm CMA}&=\int_{q_1}^{q_2}dq\int_0^{2\pi}d\phi\,\chi(\Delta E,\hat{\mathbf{q}}_n)\frac{F(q)}{E_i}\\&=\int_{q_1}^{q_2}dq\,\langle\chi(\Delta E,\theta_q(q))\rangle_\phi\frac{F(q)}{E_i}\ ,\end{aligned} \tag{A3}$$

where q_1 and q_2 are determined by the acceptance of the CMA ($\theta=42°\pm6°$) though Eq. (A1) and therefore are functions themselves of ΔE and E_i. In Eq. (A3) it is in general not possible to take average $\langle\chi\rangle$ out of the integral due to the dependence on θ_q. However, there are cases, like ours, as we shall see below, in which there is in fact no dependence at all following the combined effect of the effective dipole selection rule and the averaging on ϕ. Moreover, as a general fact, the θ_q dependence of χ comes through a Legendre polynomial $P_l^{|m|}(\cos\theta_q)$ [see Eq. (36)] which is weak any way in the range of variation of θ_q determined by the CMA. Therefore we are certainly allowed to write

$$\begin{aligned}\langle I_s(\Delta E,E_i)\rangle_{\rm CMA}&=\langle\chi(\Delta E,E_i)\rangle_{\rm CMA}\int_{q_1}^{q_2}dq\frac{F(q)}{E_i}\\&=\langle\chi(\Delta E,E_i)\rangle_{\rm CMA}\sigma_0(\Delta E,E_i)\ ,\end{aligned} \tag{A4}$$

where

$$\sigma_0(\Delta E,E_i)=\frac{1}{E_i}\int_{q_1}^{q_2}dq\,F(q)=\frac{G(\Delta E,E_i)}{E_i} \tag{A5}$$

the dependence on E_i and ΔE in the numerator G coming from q_1 and q_2.

If we indicate by $I_l(\varepsilon_p)$ the probability for the incident or scattered electron beam to loose energy ε_p due to the plasmon excitations, the observed signal $\langle I_c(\Delta E)\rangle_{\rm CMA}$ is given by

$$\begin{aligned}\langle I_c(\Delta E)\rangle_{\rm CMA}=\int_{-\infty}^{\infty}&\langle\chi(\Delta E-\varepsilon_p,E_i-\varepsilon_p\Theta(\varepsilon_p))\rangle_{\rm CMA}\\&\times\frac{G(\Delta E-\varepsilon_p,E_i-\varepsilon_p\Theta(\varepsilon_p))}{E_i-\varepsilon_p\Theta(\varepsilon_p)}\\&\times I_l(\varepsilon_p)d\varepsilon_p\ ,\end{aligned} \tag{A6}$$

where $\Theta(x)$ is the usual step function ($=1$ for $x>0$ and 0 for $x\le0$) and positive values for the losses ε_p are for the primary electron beam, whereas negative values are for the scattered beam. Due to the E_i dependence of $\langle\chi(\Delta E,E_i)\rangle_{\rm CMA}$ and $\sigma_0(\Delta E,E_i)$ this integral is not a convolution integral. However since $I_l(\varepsilon_p)$ is sizable only for $\varepsilon_p<100$ eV (see Fig. 5) we can safely neglect the plasmon loss spreading in E_i and write

$$\begin{aligned}\langle I_c(\Delta E)\rangle_{\rm CMA}\approx\sigma_0(\Delta E,E_i)\int_{-\infty}^{\infty}&\langle\chi(\Delta E-\varepsilon_p,E_i)\rangle_{\rm CMA}\\&\times I_l(\varepsilon_p)d\varepsilon_p\ .\end{aligned} \tag{A7}$$

In fact the variation of $\cos\theta_q$ due to the ε_p variation of E_i is of the order or less than $\varepsilon_p/E_i\le100/3000\approx3\%$, as can be seen from Eq. (A1), but the effect of this variation on $\langle\chi(\Delta E,E_i)\rangle_{\rm CMA}$ comes out to be less than 1%. Moreover in our case there is no explicit dependence of χ on θ_q, as already anticipated, since from Eq. (36) l and l' can be either zero or one due to the effective dipolar selection rule and

$$\begin{aligned}\langle\chi^{ll}(\Delta E,\hat{\mathbf{q}})\rangle_\phi&\approx\sum_{m,m'}{\rm Im}\tau^{00}_{lm,lm'}\int_0^{2\pi}Y_{lm}(\hat{\mathbf{q}})Y_{l'm'}(\hat{\mathbf{q}})d\phi\\&=\sum_{m=-l}^{l}{\rm Im}\tau^{00}_{lm,lm}\end{aligned} \tag{A8}$$

since in tetrahedral coordination the x, y and z direction are equivalent ($\tau^{00}_{lm,lm}$ independent of m). Note that this relation is actually valid for any l and coincides with the polarization averaged EXAFS signal in x-ray absorption.

Concerning the variation of $\sigma_0(\Delta E,E_i)$, we note that at the CMA acceptance angles $42°\pm6°$, q is about 20 Å^{-1}, which means the region over $S(q)$ in Fig. 9 is nearly constant. Since $F(q)\approx S(q)/q^3$, it is easy to

evaluate the variation of $G(\Delta E,E_i)$. One finds

$$G(\Delta E,E_i)=\int_{q_1(\Delta E,E_i)}^{q_2(\Delta E,E_i)} dq\, F(q)$$
$$\approx S(\bar{q})\int_{q_1}^{q_2}\frac{dq}{q^3}=\frac{S(\bar{q})}{2}\left[\frac{1}{q_1^2}-\frac{1}{q_2^2}\right]$$

which varies by about 1.5% on going from $E_i=3000$ eV to $E_i=2900$ eV and similarly for E_s. Therefore the biggest variation in $\sigma_0(\Delta E,E_i)$ comes from the denominator $1/E_i$ in Eq. (A5) which is 3%. Altogether we can estimate a total variation of about 4%. This finding has been corroborated by actual calculation and is in keeping with what one obtains by using the near-edge ionization formula suggested by Worthington and Tomlin [see C. J. Powell, Rev. Mod. Phys. **48**, 33 (1976) Eq. (5)] putting there $E_{nl}=E_k=1840$ eV and calculating $\sigma_{nl}(E_i)$ for $E_i=3000$ eV ($U_k=E_i/E_k=1.63$) and $E_i=2900$ eV ($U_k=1.58$).

In conclusion, with the errors indicated above, the factorization of the ionization cross section in Eq. (A7) is justified even at such relatively low incident and scattered electron energies as it is at much higher energies.[25] This fact then substantiates the kind of analysis we have performed on our date. From Eq. (A8) we see that this possibility is due to the azimuthal average performed by the CMA and the effective dipolar selection rule.

There is one last point to be discussed, namely, the assumption that the plasmon loss spectrum measured through the CMA acceptance describes the distribution of energies of the primary beam in the material. Since the production of bulk plasmon is to a very good approximation isotropic, the question is whether the measured low-loss spectrum correctly reproduces the bulk-to-surface-plasmon ratio that is present in the high-energy-loss spectrum. Now, neglecting the plasmon momentum, in the first case the surface is crossed by the electron beam at an angle of 42°±6° with respect to the normal, whereas in the second case, due to the additional momentum transfer following the ionization processes, the surface crossing can occur in the same angle range plus or minus θ_q given in Eq. (A1). This latter varies from $\theta_q=0$, for $q_n=k_i-k_s$, to $\theta_q\approx 35°=\arccos[1-(k_s/k_i)^2]^{1/2}$ for $q_n=(\Delta E)^{1/2}(k_s/k_i=1/\sqrt{3})$. Therefore to a reasonable approximation one can assume the two plasmon-loss-energy distributions with and without ionization process to be substantially similar.

*Permanent address: Dipartimento di Fisica, Università di Roma II, "Tor Vergata," 00173 Roma, Italy.

[1]M. De Crescenzi and G. Chiarello, J. Phys. C **18**, 3595 (1985), and references therein.
[2]M. De Crescenzi, F. Antonangeli, C. Bellini, and R. Rosei, Phys. Rev. Lett. **50**, 1949 (1983).
[3]A. P. Hitchcock and C. H. Teng, Surf. Sci. **149**, 558 (1985).
[4]Y. U. Idzerda, E. D. Williams, T. L. Einstein, and R. L. Park, Surf. Sci. **160**, 75 (1985).
[5]E. A. Stern, D. E. Sayers, and F. W. Lytle, Phys. Rev. B **11**, 4836 (1975).
[6]P. A. Lee, P. H. Citrin, P. Eisemberger, and B. M. Kincaid, Rev. Mod. Phys. **53**, 769 (1981).
[7]T. M. Hayes and J. B. Boyce, in *Solid State Physics,* edited by H. Ehrenreich, F. Seitz, and D. Turnbull (Academic, New York, 1982), Vol. 37.
[8]D. E. Sayers, E. A. Stern, and F. W. Lytle, Phys. Rev. Lett. **27**, 1204 (1971).
[9]M. De Crescenzi, G. Chiarello, E. Colavita, and R. Memeo, Phys. Rev. B **29**, 3730 (1984).
[10]T. Tyliszczak and P. A. Hitchcock, J. Vac. Sci. Technol. A **4**, 1372 (1986).
[11]E. Chainet, M. De Crescenzi, J. Derrien, T. T. A. Nguyen, and R. Cinti, Surf. Sci. **186**, 801 (1986).
[12]M. De Crescenzi, M. Diociaiuti, L. Lozzi, P. Picozzi, and S. Santucci, Phys. Rev. B **29**, 5997 (1987).
[13]Y. U. Idzerda, E. D. Williams, T. L. Einstein, and R. L. Park, Phys. Rev. B **36**, 5941 (1987).
[14]B. N. Kincaid, A. E. Meixner, and P. M. Platzman, Phys. Rev. Lett. **40**, 1296 (1978).
[15]R. D. Leapman, L. A. Grunes, and P. L. Fejes, Phys. Rev. B **26**, 614 (1982).
[16]W. L. Schaich, Phys. Rev. B **29**, 6513 (1984).
[17]A. Filipponi, D. Della Sala, F. Evangelisti, A. Balerna, and S. Mobilio, J. Phys. (Paris) Colloq. **47**, C8-375 (1986).
[18]A. Bianconi, A. Di Cicco, N. V. Pavel, M. Benfatto, A. Marcelli, C. R. Natoli, P. Pianetta, and J. Woicik, Phys. Rev. B **36**, 6426 (1987).
[19]F. Comin, L. Incoccia, P. Lagarde, G. Rossi, and P. H. Citrin, Phys. Rev. Lett. **54**, 122 (1985).
[20]R. D. Leapman, P. Rez, and D. F. Mayers, J. Chem. Phys. **72**, 1232 (1980).
[21]F. Mila and C. Noguera, J. Phys. C **20**, 3863 (1987).
[22]M. J. Mehl and T. L. Einstein, Phys. Rev. B **36**, 9011 (1987).
[23]D. K. Saldin, Phys. Rev. Lett. **60**, 1197 (1988).
[24]C. Brouder, M. F. Ruiz Lopez, R. F. Pettifer, M. Benfatto, and C. R. Natoli, Phys. Rev. B **39**, 1488 (1989).
[25]R. D. Leapman, L. A. Grunes, P. L. Fejes, and J. Silcox, in *EXAFS Spectroscopy: Techniques and Applications,* edited by B. K. Teo and D. C. Joy (Plenum, New York, 1981), p. 217.
[26]L. I. Johansson and I. Lindau, Solid State Commun. **29**, 379 (1979); G. D. Mahan, Phys. Status Solidi B **55**, 703 (1973).
[27]B. K. Teo and P. A. Lee, J. Am. Chem. Soc. **101**, 815 (1979).
[28]N. F. Mott and H. S. W. Massey, *The Theory of Atomic Collisions,* 3rd ed. (Oxford University Press, Oxford, 1965).
[29]H. A. Bethe and R. Jackiw, *Intermediate Quantum Mechanics,* 3rd ed. (Benjamin Cummings, Menlo Park, California, 1986).
[30]J. B. Pendry, *Low Energy Electron Diffraction* (Academic, London, 1974).
[31]M. A. Van Hove, W. H. Weinberg, and C. M. Chan, *Low Energy Electron Diffraction* (Springer-Verlag, Berlin, 1986).
[32]M. Benfatto and C. R. Natoli (unpublished).
[33]V. I. Ochkur, Zh. Eksp. Fiz. **47**, 1746 (1964) [Sov. Phys.—JETP **20**, 1175 (1965)].
[34]R. Zeller, J. Phys. C **20**, 2347 (1987).
[35]H. Froitzheim, *Electron Energy Loss Spectroscopy,* in *Electron Spectroscopy for Surface Analysis,* edited by H. Ibach (Springer-Verlag, Berlin, 1981), p. 205.
[36]N. R. Avery, Surf. Sci. **111**, 358 (1981).
[37]A. G. Nassiopoulos and J. Cazaux, Surf. Sci. **149**, 313 (1985).
[38]M. Benfatto, C. R. Natoli, A. Bianconi, J. Garcia, A. Marcelli, M. Fanfoni, and I. Davoli, Phys. Rev. B **34**, 5774 (1986).
[39]L. Mattheis, Phys. Rev. **134**, A970 (1964).